Evaluation of Manning's Coefficients for the Al-Adhaim River Basin in Iraq utilizing Modern Techniques

Faris Sahib Alrammahi
Department of Engineering, Imam Al-Kadhim College, Baghdad, Iraq
farisali@iku.edu.iq (corresponding author)

Qais Hatem Mohammed Al-Madhlom
Department of Automobile Engineering, Faculty of Engineering/ Al-Musayab, University of Babylon, Hilla, Iraq
met.qais.hatem@uobabylon.edu.iq

Sanaa Abdulrazaq Jassim
Department of Energy & Renewable Energy Engineering, Faculty of Engineering/ Al-Musayab, University of Babylon, Hilla, Iraq
met.sanaa.abd@uobabylon.edu.iq

Received: 14 January 2025 | Revised: 7 February 2025 | Accepted: 9 February 2025

 DOI: https://doi.org/10.48084/etasr.10246

ABSTRACT

The current study presents an innovative analysis that combines climate and land use data to assess changes in Manning's coefficient within the Al-Adhaim River Basin (ARB) from 2017 to 2023. The primary objective is to calculate the hydraulic roughness coefficient (Manning coefficient, n) and evaluate its variations in relation to climate and land use changes. The ArcGIS and HEC-RAS software were utilized for the spatial and hydraulic analysis, respectively, as well as to calculate the arithmetic average for the entire study area. The results indicate an increase in temperature, humidity, and rainfall of 0.82 °C, 1.07 g/kg, and 0.41 mm/year, respectively, with a decrease in wind speed of 0.02 m/s. These climatic changes contributed to a 3.96% increase in crop area, while human activities led to a 0.72% rise in built areas and a 3.93% reduction in open areas. Manning's coefficient, despite its low value of 0.0695, demonstrated a strong relationship between its value and the aforementioned factors.

Keywords-Al-Adhaim; Manning's coefficient; ArcGIS; HEC-RAS; land use; land cover; climate change

I. INTRODUCTION

In recent years, Iraq has been facing challenges in water management caused by both internal and external factors [1]. At the local level, there has been a decline in the national water reserve and an increase in the need for water due to the population growth and the variety of life requirements. At the external level, the construction of dams in Iran and Turkey, as well as the decline in the amount of Euphrates River water coming from Syria, has contributed to this situation. Therefore, there is a need to study the available opportunities for optimal water management. Since Al-Adhaim River Basin (ARB) is considered the most important basin feeding the Tigris River, as well as the only basin whose catchments are from sub-basins in Iraq, this research aims to investigate it closely.

Many hydraulic properties greatly affect the water flow on the surfaces of river basins, whether these surfaces are man-made or natural. Similarly, several physical properties are modified owing to some factors, the most important of which are erosion, sediments, construction work, agriculture, etc.[1]. Among these hydraulic factors, the Manning coefficient (n), acts as an indicator of channel's roughness, significantly affecting the flow velocity.

Following the publication of (1) in 1889 [2], scientist Robert Manning significantly transformed the understanding of water dynamics and flow velocity. This equation was adopted in the design of open-flow channels and other applications, resulting in notable advancements in water management.

$$V = \frac{1}{n} R^{2/3} S^{1/2} \quad (1)$$

where V is the stream-velocity (m/s), R is the hydraulic-radius (m), which is the result of dividing the cross-area of the channel by its wetted circumference, and S is the hydraulic-

gradient, whether it represents the energy gradient or the slope of the channel bed.

The n coefficient depends significantly on the quality of land surface in terms of cover and use, known as Land Use and Land Cover (LULC). The concept is: the smoother the surface, the lower the n value, and the other way around. Therefore, any change in LULC is reflected in the land's roughness and in n value. Additionally, any adjustment in this coefficient affects the flow rate and thus the amount of water flowing in the watercourse or river. The importance of calculating coefficient n has been highlighted in various researches. A specialized guide was developed for this coefficient based on the characteristics related to the flow surface and soil types, as demonstrated in the guide by authors in [3], in cooperation with the Ministry of Transportation and the Public Highway Administration of USA. Afterwards, attempts were developed to estimate the n values considering factors such as climatic conditions [4-5]. Both studies demonstrated the importance of n values and their impact on the applied methods and climatic factors. It is evidenced that n is greatly affected by land use and vegetation cover in many studies, including the research in [6], where the clear effect of increasing the change in the vegetation surface by increasing the n values was mentioned. In [7], authors indicated negative effects on water distribution and flow through rainfall rates and some other hydrological factors. Authors in [8] evaluated the influence of climate change on water quality in the ARB utilizing the SWAT model. Additionally, authors in [9] investigated the impact of climate change on water flows in the Hunza Basin of the Himalayas employing the PREVAH model. The findings indicated that a change in temperature would significantly increase glacier melt runoff and subsequently increase total stream runoff.

Population growth and shifts in land use have resulted in soil erosion and changes in land use patterns, impacting the n values [10-11]. Additionally, the development of the digital world and the use of satellites in various scientific fields have resulted in the progress of modern methods for estimating n values, with remote sensing images being the most effective technique. Authors in [12] demonstrated the validity of satellite images for estimating n values, while authors in [13] utilized a different type of satellite imagery, known as Synthetic Aperture Radar (SAR), to enhance the hydrological model and n coefficient associated with the flow and movement of small water branches. In 2019, the effectiveness of satellite images (Landsat 8) was demonstrated in hydrological and environmental modeling [14], employing remote sensing data to develop estimation models for water quality indicators with high accuracy (R^2~96.8%).

As for the evaluation of hydrological and hydraulic models, several researches have been developed. Authors in [15] estimated the ArcSWAT model in analyzing the Diyala River Basin at the Hamrin Dam area in Iraq. Similarly, in [2, 16] the HEC-HMS model was examined in two regions of Iraq. In 2022, hydraulic models such as HEC-RAS model and WRF-Hydro model have been validated studying the flood patterns of the Khazir River in northern Iraq and in Brazil, respectively [17, 18]. In 2024, the HEC-RAS model was developed using neural networks, to examine the hydraulics of the Diyala River Basin [19]. Authors in [20] developed a modern technique investigating floods that can perform at large scales. The experimental results for the 2022 Pakistan flood demonstrate that the proposed method enables high-precision. A comparison between two types of satellite data was verified in hydrological models [21].

These researches highlight a clear gap in the study of ARB, especially with regard to the important factor, n. Hence, this study seeks to achieve a spatial-temporal analysis of ARB and the extent of the relationship with climate change and LULC in the period from 2017 to 2023 utilizing advanced techniques of remote sensing images, ArcGIS, and HEC-RAS software.

II. METHODOLOGY

A. Study Area

The Tigris River includes many tributaries, whether permanent or seasonal. Among these, the most important is the ARB, situated in the northeastern Iraq. The study area has a surface of approximately 13,000 km^2 positioned between longitudes 44.5° E and 45° E, and latitudes 34.5° N and 35° N [2].This basin is surrounded by mountainous regions with the Hamrin Mountains rising to 800 meters above sea level to the north, and lower in elevation to the west. The southeast side slopes down to plains at 150 meters above sea level, leading towards Baghdad, the capital of Iraq. Figure 1 illustrates the location of the study area.

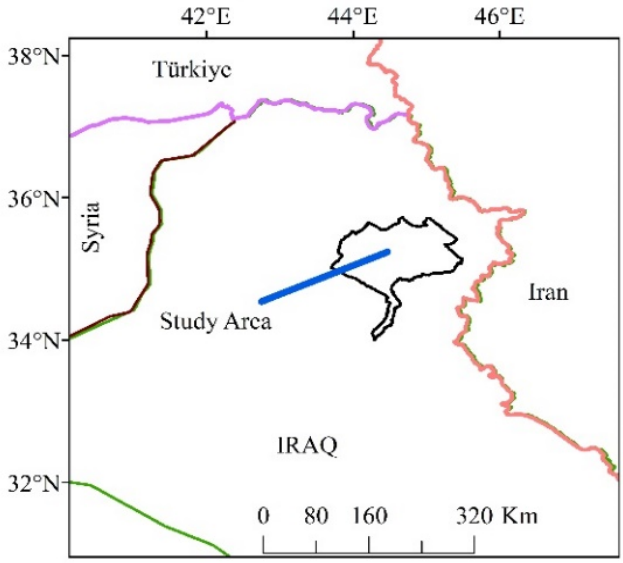

Fig. 1. Location of study area (ARB) in Iraq.

The climate in the region ranges from arid to semi-arid. The water year, similar to most areas of Iraq, starts in October and concludes around May [16]. Water flow peaks during winter, depending on annual rainfall that varies between 250 to 400 mm, while temperatures can reach less than 10 ^oC. In contrast, summer temperatures can exceed 45 ^oC leading to a decrease in water availability. The Al-Adhaim River, originating from the basin, is notable for its numerous branches, and it is supported

by a network of dams, regulators, and channels designed for storage, irrigation, and various human uses [2].

B. Materials and Methods

The current research aims to evaluate the n coefficient requiring several data and software obtained from reliable official websites and sources, as follows:

- Remote sensing images

The Digital Elevation Method (DEM), downloaded from NASA website, was utilized to determine the location and terrain data of the study area while Arc-GIS software (version 10.3) was used to capture the study area.

- Climate data

The climate analysis of the study area utilized data from the Iraqi Ministry of Environment and the NASA climate data website, for the years 2017 to 2023. Four important factors were considered: temperature, rainfall, relative humidity, and wind speed. These factors were derived from the research findings outlined in the prior section.

- Satellite images of LULC:

All LULC images of the study area were downloaded from the official website of Sentinel-2 for the study period of 2017-2023, with an accuracy of up to an altitude of 12 to 30 m.

- Soil Types of study area:

The soil type was determined through a combination of remote sensing images and FAO data, utilizing the official FAO software, the HWSD Viewer. Once the soil type codes were obtained, they were cross-referenced with published indices to accurately determine the corresponding soil types.

The HEC-RAS (version 6.1) is crucial for this study as it enables the extraction of n values with high accuracy by analyzing topographic and land use data and correlating them with the hydraulic properties of the ARB. After obtaining DEMs and LULC images from NASA and Sentinel-2 satellite data, the information is processed using ArcGIS which facilitates the determination of standard. All data is then transferred to HEC-RAS to calculate the n values. This process is continued by linking these classifications with the soil information derived from the HWSD Viewer database, thus classifying them according to the standard values listed in the Table I [3].

The HEC-RAS program calculates the n values according to these standard values and matches them with the soil and LULC data for each part of the study area. These operations are carried out for each year of the study period, and after each year, the data are transferred to ArcGIS again to represent and draw them in point form.

These results were analyzed to be plotted according to the mathematical data of Arc-GIS. The average of the n values was calculated using the following formula:

$$Average\ (n) = \frac{\sum n * a}{\sum a} \quad (2)$$

where a is the area of each element with similar surface-type.

TABLE I. APPROVED MANNING'S COEFFICIENT ACCORDING TO THE LAND COVER [3]

Surface type details	*n* values
Unclassified (default value used)	0.03
Developed-high intensity	0.11
Developed-medium-intensity	0.1
Developed-low-intensity	0.05
Developed-open-space	0.02
Cultivated-crops	0.037
Pasture	0.045
Grassland-herbaceous	0.034
Deciduous forest	0.1
Evergreen forest	0.11
Mixed forest	0.1

III. RESULTS AND DISCUSSION

A. Remote Sensing Image Extraction

Figure 2 illustrates the satellite image (DEM) of the study area which extracted using ArcGIS software.

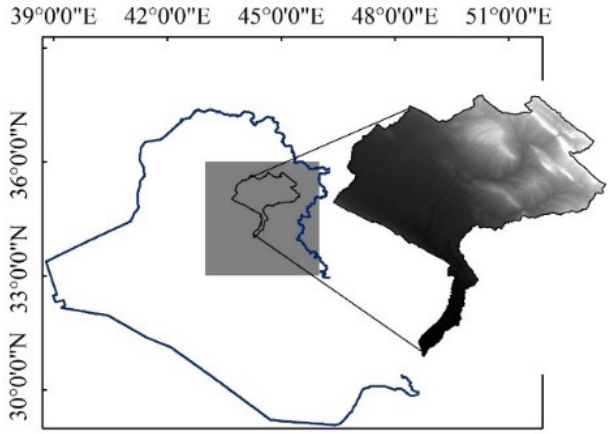

Fig. 2. Satellite image of the study area.

B. Analysis of Climate Factors

Figure 3 depicts the maximum and average precipitation levels in the study area. The region experiences the highest rainfall, ranging from 27 to 55 mm/day, with peak values recorded in February and March each year. In contrast, the average rainfall ranges from 0.5 to 1 mm per day. It is important to note that during the summer season, the average rainfall drops to zero, reflecting the area's arid climate.

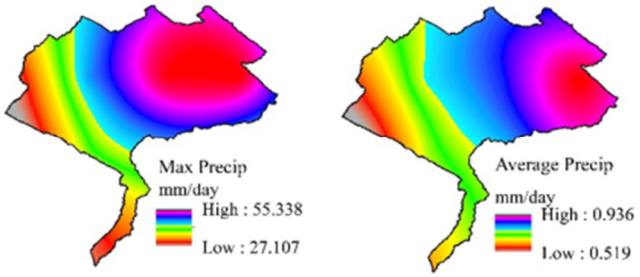

Fig. 3. Maximum and average precipitation levels in ARB region.

Generally, the specific humidity in ARB area varies greatly between summer and winter while it is moderate in spring and autumn. This was confirmed by analyzing the humidity data in this region (Figure 4), where the maximum specific humidity is observed at 12 g/kg and the minimum at 1.3 g/kg (usually in cold weather).

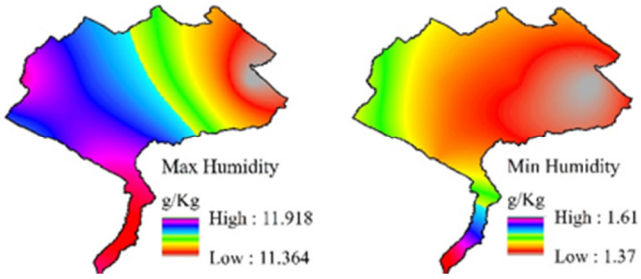

Fig. 4. Maximum and average humidity values in ARB.

Wind speed also changes between winter and summer, with higher values recorded in winter and lower in summer. Figure 5 indicates that the maximum wind speed was around 10 m/s and the lowest value was 1 m/s. The closer you get to the center of the region, the stronger the wind is.

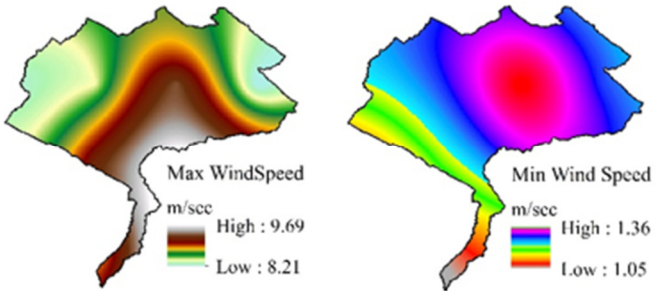

Fig. 5. Maximum and average values of wind speed in ARB.

Figure 6 presents the maximum and average levels of temperature captured in ARB area. Specifically, in winter temperature drops below zero degrees Celsius at night, while during the day it ranges between 10 to 15 ^{o}C. During spring, temperature ranged from 21 to 31 ^{o}C, contributing to the growth of herbs and plants. The highest temperatures each year are observed in summer (43-48 ^{o}C), while the lowest temperatures were recorded approximately at -5 ^{o}C.

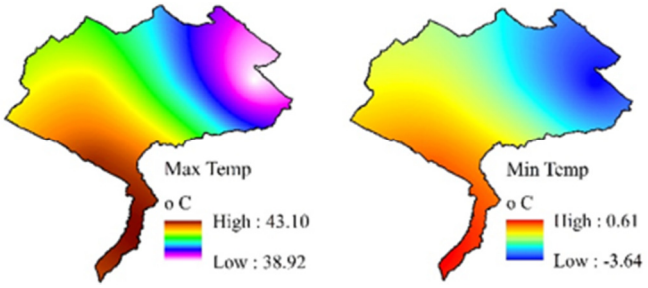

Fig. 6. Maximum and average temperature values in ARB region.

C. Classification of Land Cover/Use

According to the results of previous researches, the method of land use and its distribution was crucial in understanding the movement and flow of surface runoff water (through its effect on the Manning number). Therefore, land use was accurately classified into its types using satellite images and modern techniques described previously. The findings contained seven main categories, as presented in Figures 7-13.

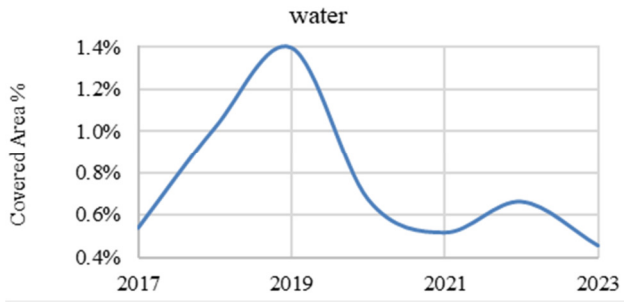

Fig. 7. Evolution of water-covered area percentage from 2017 to 2023.

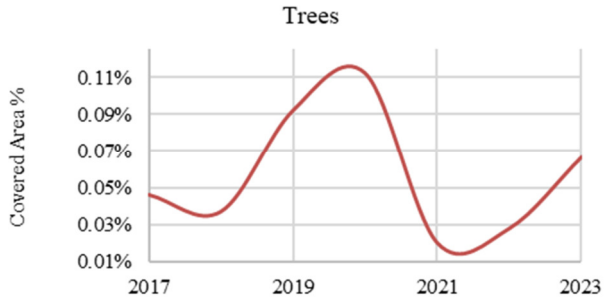

Fig. 8. Evolution of tree-covered area percentage from 2017 to 2023.

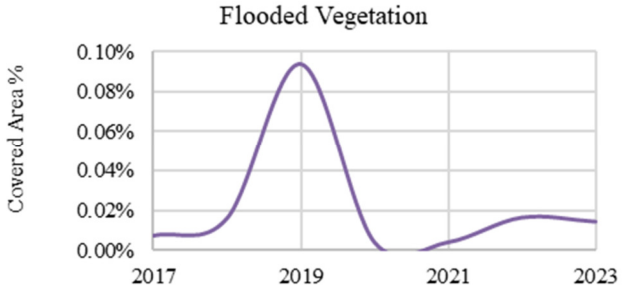

Fig. 9. Evolution of flooded vegetation-covered area percentage from 2017 to 2023.

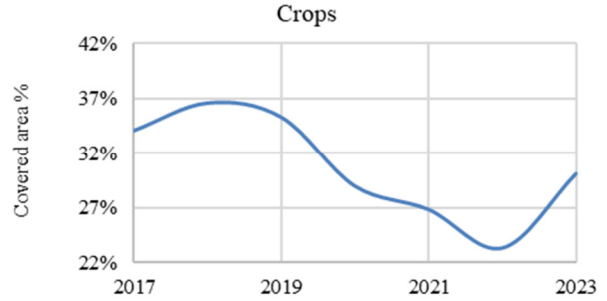

Fig. 10. Evolution of crops-covered area percentage from 2017 to 2023.

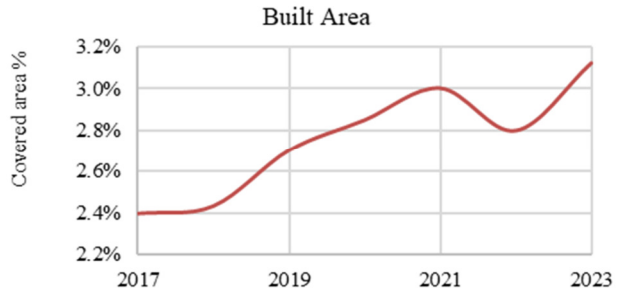

Fig. 11. Evolution of built-covered area percentage from 2017 to 2023.

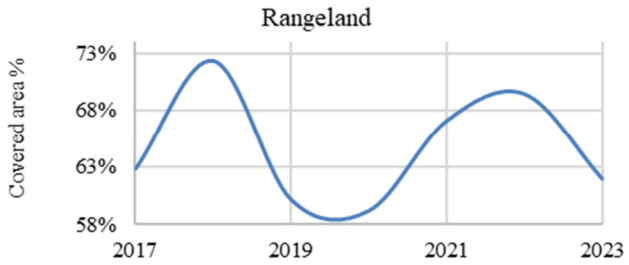

Fig. 12. Evolution of rangeland-covered area percentage from 2017 to 2023.

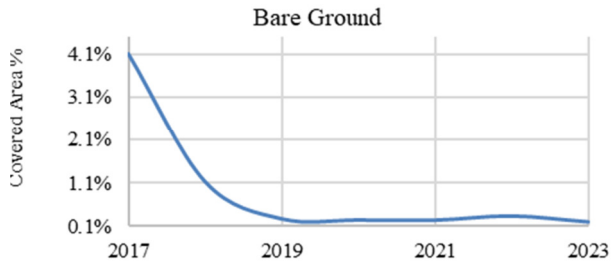

Fig. 13. Evolution of bare ground-covered area percentage from 2017 to 2023.

D. Classification of Soil

The study area contained seven kinds of soil types, classified according to their respective codes, as presented in Table II. After matching the codes with their corresponding soil types and regrouping them according to their similarities, three soil types were classified again, as shown in Table III.

TABLE II. CLASSIFICATION OF SOIL TYPES CODES FOR ARB

Soil Type Code	Covered area (m^2)	Percentage %
3136	92031196.5	0.7%
3298	604156911.7	4.8%
3300	4601530046	36.7%
3312	1876794986	15.0%
3323	322843325.8	2.6%
3324	1696107336	13.5%
3561	611937311.8	4.9%
3603	2226851947	17.8%
3614	49683979	0.4%
3616	94070179.9	0.8%
3627	358742902.7	2.9%

Figure 14 provides an alternative perspective on the soil types in the study area, illustrating their coverage percentages based on established classification systems. These classifications include properties such as salinity, alkalinity, and other scientific arrangements.

TABLE III. ARB SOIL TYPE CLASSIFICATION AND RATIO OF THE COVERED AREA

USDA Field	Covered area (m^2)	Percentage
clay	611937311.8	5%
clay loam	358742902.7	3%
loam	11564069908	92%

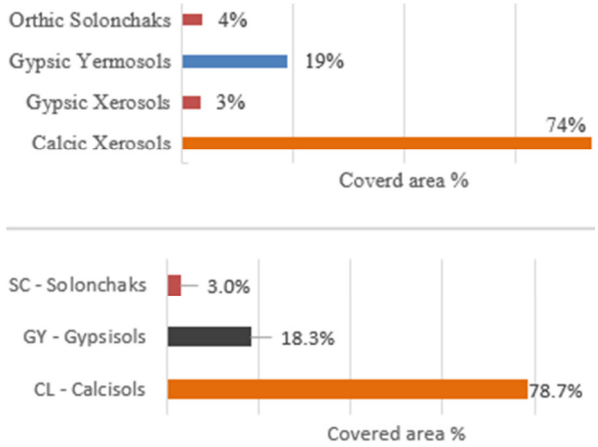

Fig. 14. Alternative scientific classification of soil types in the study area.

E. Manning Values for the Study Period

By applying modern techniques described in this research to match soil type data and land cover data, the results, as shown in Table IV, revealed seven surface types in the study area (Figures 15-21).

TABLE IV. CLASSIFICATION SURFACE TYPE FOR ARB ACCORDING TO THE STANDARD ONES [3]

Cover-Type with code	Manning's coefficient
1-Unclassified land-cover	0.03
2-Developed High-Intensity land-cover	0.11
4-Developed Low-Intensity land-cover	0.05
5-Developed Open-Space land-cover	0.02
7-Pasture Hay land-cover	0.045
8-Grassland Herbaceous land-cover	0.034
11-Mixed Forest land-cover	0.1

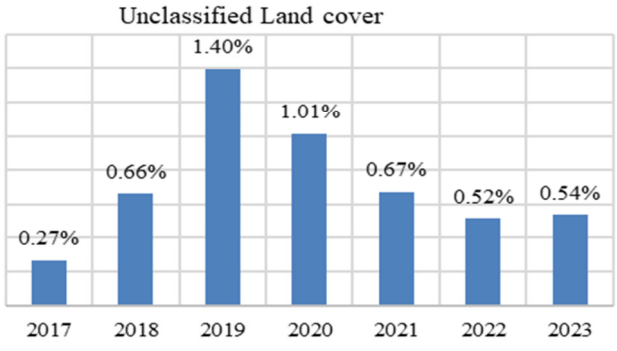

Fig. 15. Percentage of unclassified land cover type through the study period.

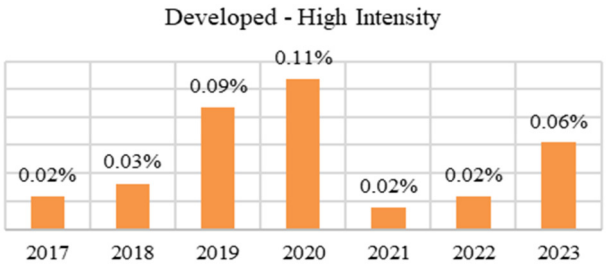

Fig. 16. Percentage of developed-high intensityland cover type through the study period.

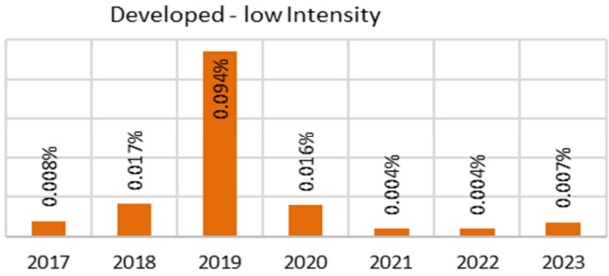

Fig. 17. Percentage of developed-low intensity land cover type through the study period.

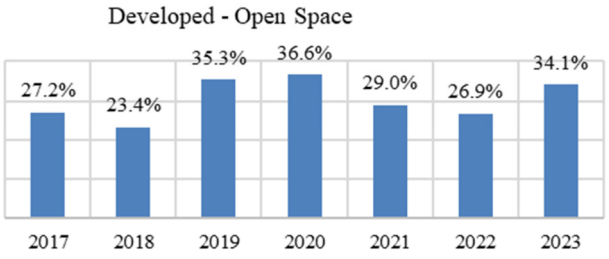

Fig. 18. Percentage of developed-open spaceland cover type through the study period.

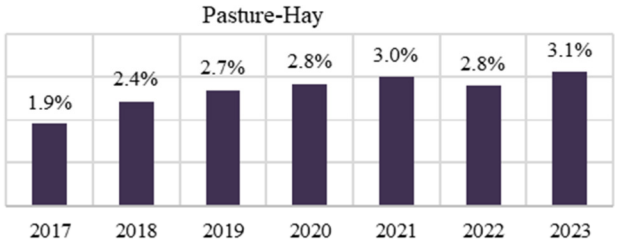

Fig. 19. Percentage of pasture-hay land cover type through the study period.

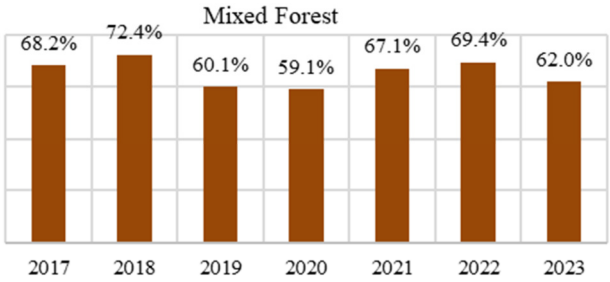

Fig. 20. Percentage of pasture-hay land cover type through the study period.

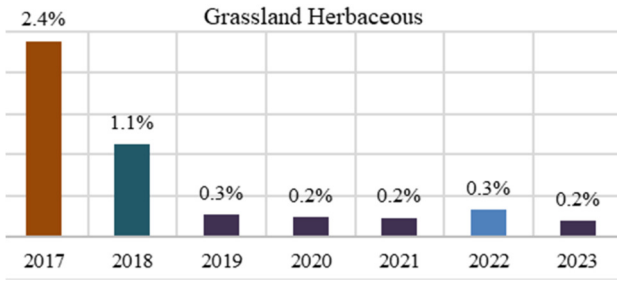

Fig. 21. Percentage of grassland-herbaceousland cover type through the study period.

The results clearly indicate changes across all surface types, reflecting their impact on the total *n* value rates over the course of one year, as shown in Figure 22-28.

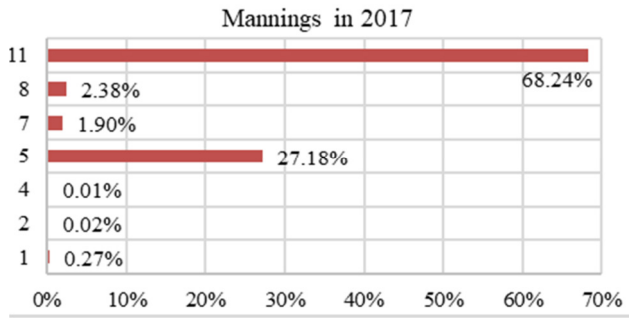

Fig. 22. Surface types with their percentages covered for ARBin 2017.

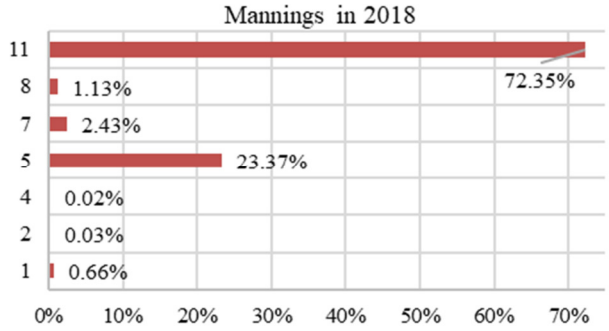

Fig. 23. Surface types with their percentages covered for ARBin 2018.

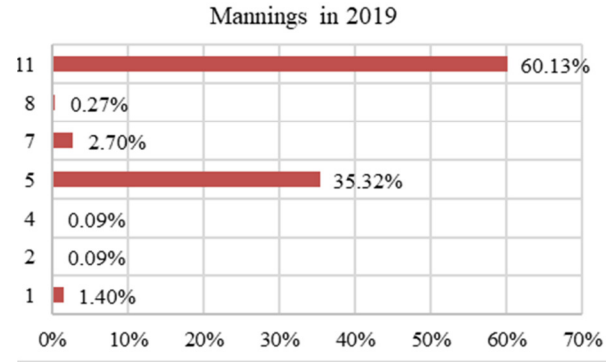

Fig. 24. Surface types with their percentages covered for ARBin 2019.

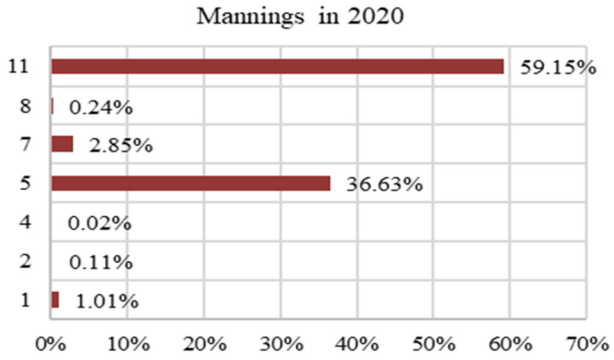

Fig. 25. Surface types with their percentages covered for ARBin 2020.

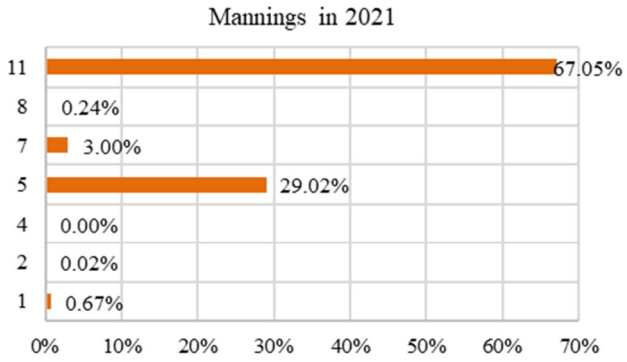

Fig. 26. Surface types with their percentages covered for ARBin 2021.

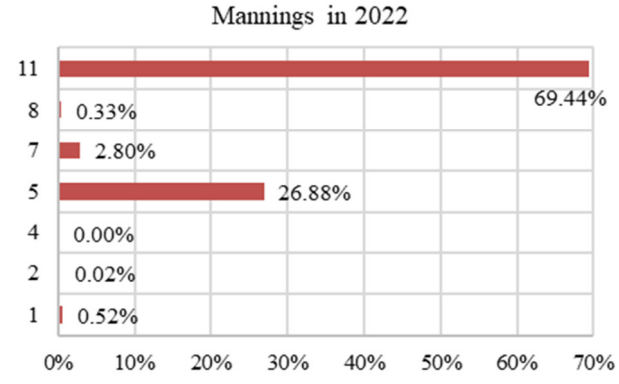

Fig. 27. Surface types with their percentages covered for ARBin 2022.

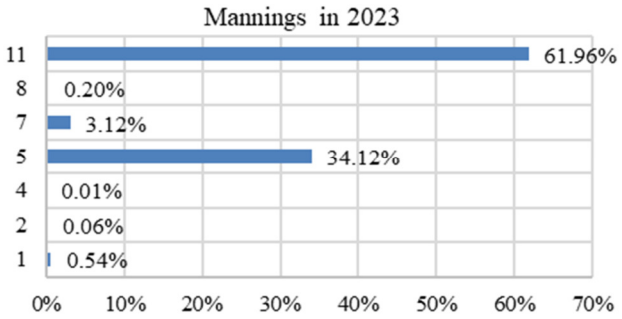

Fig. 28. Surface types with their percentages covered for ARBin 2023.

F. Evaluation and Linking Results of Manning's Values

The analysis of the results for the four climate elements from 2017 to 2023 indicates a notable increase in temperatures, humidity, and annual precipitation rates in the study area with values of approximately 0.82 °C, 1.07 g/kg, and 0.41 mm/year, respectively. In comparison, the average wind speed noted a decrease of 0.02 m/s, as illustrated in Figure 29.

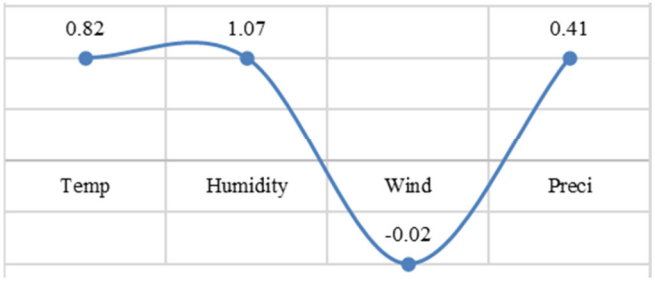

Fig. 29. Differences in Climate Factors from 2017 to 2023.

The increase in the aforementioned temperatures, as well as specific humidity and annual precipitation rates, performed a key role in the potential growth of vegetation cover and thus impeding water flow (increasing the values of n). In contrast, decreasing wind speed leads to the possibility of the soil surface maintaining its texture without any effect of rapid erosion factors and thus stabilizing the values of n. Table V presents the changes of climatic factors between 2017 and 2023, at the beginning and ending of the study period.

TABLE V. DIFFERENCE IN CLIMATE FACTORS BETWEEN 2017 AND 2023

Year	T (°C)	Humidity (g/kg)	Wind speed (m/s)	Precipitation (mm/day)
2017	21.5	9.5	3.0	350
2023	22.3	10.57	2.98	390

The impact of climatic factors can be analyzed both individually and in combination. Increased temperatures have resulted to increased evaporation rates and vegetation cover, thus leading to increased n values in some areas. Additionally, the recorded rise in the annual precipitation rate changed soil's nature and modified the properties of hydraulic flow. In terms of relative humidity's increase, which has contributed to an increase in surface roughness, especially in agricultural areas, (increase in n value). Furthermore, a reduction in wind speed has helped decrease erosion rates in some areas, thereby preserving the stability of n values. This correlation between these factors and the changes that occurred in vegetation cover using satellite images, allowed a deeper understanding of the impact of climate change on the roughness of water channels in the basin. These findings underscore the necessity for developing integrated water resource management strategies that consider the escalating impacts of climate change.

When comparing the covered areas with the types of land surfaces explained previously, it became clear that there were percentages that increased (e.g., building areas 0.72%) and percentages that declined (e.g., Bare ground, 3.93%), as illustrated in Figure 30. After calculating the average n values

during the study period, the results demonstrated a consistent change Ultimately, the final average for the entire study basin stabilized at 0.0705, as illustrated in Figure 31.

Figure 32 illustrates the change in Manning's coefficients over the time period 2017-2023. The variations in the individual n values reflected the extent to which they are affected by climatic factors and types of land surfaces. The decline in the n values in 2019-2023 is related to the increase in the intervention of building areas and the decrease in open areas.

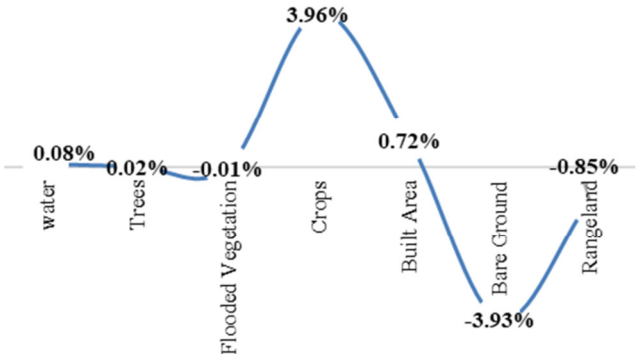

Fig. 30. Variation of land use percentages through the study period of 2017-2023.

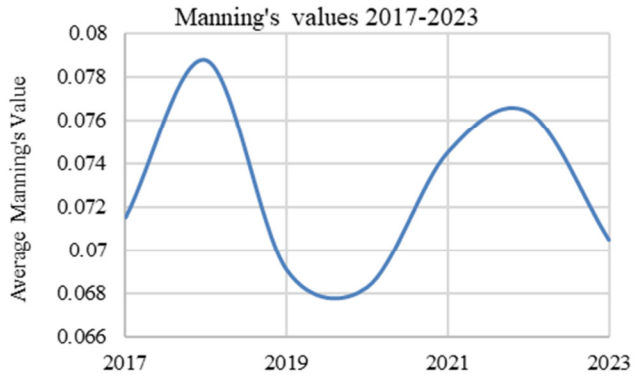

Fig. 31. Variation of average Manning's n values (2017-2023).

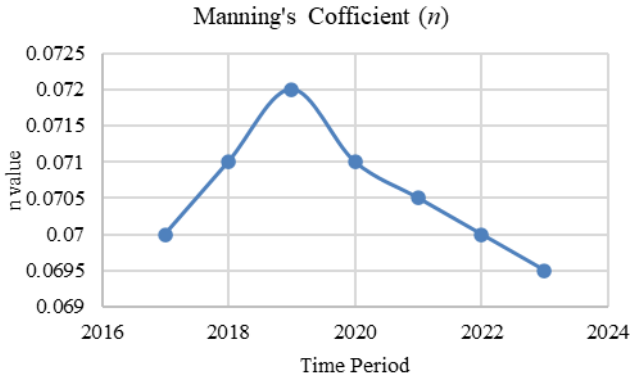

Fig. 32. Variation of Manning's n values (2017-2023).

IV. CONCLUSION

This study presents a comprehensive analysis of the variation in Manning's coefficient (n) in the Al-Adhaim River Basin (ARB), focusing on the effects of land use during the period 2017-2023, as well as the corresponding changes in climatic factors. Despite the hydrological importance of the basin, there is still a research gap in understanding the interrelationship between surface changes, climate changes, and n in a highly variable environment such as Iraq. The research aims to fill this gap by integrating satellite image analysis with modern techniques.

It was evident that:

- Any change in the surface's type and climatic factors has a direct effect on the average values of n for the entire ARB region.
- The growth of vegetation cover (crops) resulted in a rise in the individual values of n coefficient.
- The significant expansion of building areas, correlated to a reduction the open areas (e.g., Bare ground) resulted in a decrease in the values of n.

The results of this study are consistent with the findings of [10], regarding the impact of human activities in Iraq, and support the validity of utilizing satellite images in the analysis of surface changes, as pointed out by [13]. However, this study differs from previous research by integrating temporal and spatial analysis of n values using modern techniques such as HEC-RAS and ArcGIS to provide a more accurate view of the relationship between climate change and surface changes. The researchers suggest several proposals for future research to ensure development in obtaining more accurate estimates to reach effective water management. These include:

- Monitoring additional climatic factors to improve accurate predictions and optimize water management strategies in the study area.
- Developing strategies to manage the expansion of building areas that affect water movement within the region.
- Increasing awareness of climatic factors risks and changes in land surfaces on water management

REFERENCES

[1] F. Alrammahi, S. Khassaf, S. Abbas, H. Madhloom, M. Aljaradin, and N. Al-Ansari, "Study the slope stability of earthen dam using dimensional analysis techniques," *International Journal of GEOMATE*, vol. 21, no. 83, pp. 125–131, 2021.

[2] A. N. A. Hamdan, S. Almuktar, and M. Scholz, "Rainfall-Runoff Modeling Using the HEC-HMS Model for the Al-Adhaim River Catchment, Northern Iraq," *Hydrology*, vol. 8, no. 2, Jun. 2021, Art. no. 58, https://doi.org/10.3390/hydrology8020058.

[3] G. J. Arcement and V. R. Schneider, "Guide for selecting Manning's roughness coefficients for natural channels and flood plains" United States Geological Survey, 2339, 1989, https://doi.org/10.3133/wsp2339.

[4] D. T. Soong, T. M. Halfar, M. A. Jupin, and L. A. Wobig, "Methods for Determining Manning's Coefficients for Illinois Streams," pp. 1–12, Apr. 2012, https://doi.org/10.1061/40737(2004)188.

[5] A. E. Harka, N. T. Roba, and A. K. Kassa, "Modelling rainfall runoff for identification of suitable water harvesting sites in Dawe River

watershed, Wabe Shebelle River basin, Ethiopia," *Journal of Water and Land Development*, no. 47, pp. 186–195, 2020, https://doi.org/10.24425/jwld.2020.135313.

[6] R. García Díaz, "Analysis of Manning coefficient for small-depth flows on vegetated beds," *Hydrological Processes*, vol. 19, no. 16, pp. 3221–3233, 2005, https://doi.org/10.1002/hyp.5820.

[7] A. J. Shaaban, M. Z. M. Amin, Z. Q. Chen, and N. Ohara, "Regional Modeling of Climate Change Impact on Peninsular Malaysia Water Resources," *Journal of Hydrologic Engineering*, vol. 16, no. 12, pp. 1040–1049, Dec. 2011, https://doi.org/10.1061/(ASCE)HE.1943-5584.0000305.

[8] N. Abbas, S. A. Wasimia, and N. Al-Ansari, "Assessment of Climate Change Impact on Water Resources of Lesser Zab, Kurdistan, Iraq Using SWAT Model," *Engineering*, vol. 8, pp. 697–715, 2016.

[9] A. N. Laghari, W. Rauch, and M. A. Soomro, "A hydrological response analysis considering climatic variability," *Engineering, Technology & Applied Science Research*, vol. 8, no. 3, pp. 2981–2984, 2018.

[10] V. K. Sissakian, Z. Elias, and N. Al-Ansari, "Soil Erosion in Al-Adhaim River Basin, Central Part of Iraq" Research Square, Aug. 10, 2023, https://doi.org/10.21203/rs.3.rs-3235826/v1.

[11] R. Z. Harifidy, I. Hiroshi, R. Z. M. Harivelo, M. Jun, S. Kazuyoshi, and M. Keiichi, "Assessing future intra-basin water availability in madagascar: Accounting for climate change, population growth, and land use change," *Water Research*, vol. 257, Jun. 2024, Art. no. 121711, https://doi.org/10.1016/j.watres.2024.121711.

[12] G. Forzieri, G. Moser, E. R. Vivoni, F. Castelli, and F. Canovaro, "Riparian Vegetation Mapping for Hydraulic Roughness Estimation Using Very High Resolution Remote Sensing Data Fusion," *Journal of Hydraulic Engineering*, vol. 136, no. 11, pp. 855–867, Nov. 2010, https://doi.org/10.1061/(ASCE)HY.1943-7900.0000254.

[13] A. Tarpanelli, L. Brocca, F. Melone, and T. Moramarco, "Hydraulic modelling calibration in small rivers by using coarse resolution synthetic aperture radar imagery," *Hydrological Processes*, vol. 27, no. 9, pp. 1321–1330, 2013, https://doi.org/10.1002/hyp.9550.

[14] M. V. Japitana and M. E. C. Burce, "A satellite-based remote sensing technique for surface water quality estimation," *Engineering, Technology & Applied Science Research*, vol. 9, no. 2, pp. 3965–3970, 2019.

[15] T. S. Khayyun, I. A. Alwan, and A. M. Hayder, "Hydrological model for Hemren dam reservoir catchment area at the middle River Diyala reach in Iraq using ArcSWAT model," *Applied Water Science*, vol. 9, no. 5, Jul. 2019, Art. no. 133, https://doi.org/10.1007/s13201-019-1010-0.

[16] F. S. Alrammahi and A. N. Ahmed Hamdan, "Simulation of Rainfall-Runoff in the Diyala River Basin in Iraq using Hydrological Model by HMS with remote sensing, Geo-HMS and ArcGIS," *IOP Conference Series: Earth and Environmental Science*, vol. 1120, no. 1, Sep. 2022, Art. no. 012007, https://doi.org/10.1088/1755-1315/1120/1/012007.

[17] A. A. M. AL-Hussein, S. Khan, K. Ncibi, N. Hamdi, and Y. Hamed, "Flood Analysis Using HEC-RAS and HEC-HMS: A Case Study of Khazir River (Middle East—Northern Iraq)," *Water*, vol. 14, no. 22, Jan. 2022, Art. no. 3779, https://doi.org/10.3390/w14223779.

[18] D. G. Silva *et al.*, "WRF-Hydro for Streamflow Simulation in the MATOPIBA Region within the Tocantins/Araguaia River Basin—Brazil: Implications for Water Resource Management," *Water*, vol. 15, no. 22, Jan. 2023, Art. no. 3902, https://doi.org/10.3390/w15223902.

[19] F. S. Alrammahi and A. N. A. Hamdan, "Hydraulic model for flood inundation in Diyala River Basin using HEC-RAS, PMP, and neural network," *Open Engineering*, vol. 14, no. 1, Jan. 2024, https://doi.org/10.1515/eng-2022-0530.

[20] Q. Xu, Y. Shi, J. L. Bamber, C. Ouyang, and X. X. Zhu, "Large-scale flood modeling and forecasting with FloodCast," *Water Research*, vol. 264, Oct. 2024, Art. no. 122162, https://doi.org/10.1016/j.watres.2024.122162.

[21] M. S. Sh, J. A. Tabark, and J. M. Atyaf, "Comparison Between Satellite Rainfall Data and Dain Gauge Stations in The Al-Adhaim Watershed, Iraq," *Plant Archives*, vol. 20, no. 2, pp. 625–629, 2020.